PERGAMON

Journal of Asian Earth Sciences 19 (2001) 85–95

Journal of Asian Earth Sciences

www.elsevier.nl/locate/jseaes

$^{40}Ar/^{39}Ar$, pressure, temperature and fission track constraints on the age and nature of metamorphism around the main central thrust in the eastern Bhutan Himalaya

K. Stüwe[a,*], D. Foster[b]

[a]*Institut für Geologie und Paläontologie, Universität Graz, Heinrichstr. 26, A-8010, Graz, Austria*
[b]*Department of Geology, University of Florida, Gainesville, FL, 32611, USA*

Abstract

$^{40}Ar/^{39}Ar$ data from a profile across the Main Central Thrust in the eastern Bhutan Himalaya indicate muscovite cooling ages of 14.1 ± 0.2 Ma from a sample in the immediate hanging wall of the thrust and 11.2 Ma from about 400 m structurally higher in the hanging wall. These two ages are repeated by two samples from 2.1 and 4.7 km vertical distance from the thrust within the hanging wall, respectively. A single apatite fission track age from the immediate hanging wall of the thrust gives an age of 3.1 ± 0.6 Ma. Pressure–temperature estimates give temperatures around 650°C and 6.5 kbar for the highest sample collected. Samples closer to the Main Central Thrust give also temperatures between 600 and 650°C at the same pressure, indicating possibly a slight temperature decrease with proximity to the thrust. However, uncertainties are large and the parageneses are thermodynamically too highly variant to place much significance on their interpretation.

The $^{40}Ar/^{39}Ar$ cooling age data are consistent with a repetition of the sequence in the hanging wall of the thrust. They confirm the data of Davidson et al. (1997; Metamorphic reactions related to decompression and synkinematic intrusion of leucogranite, High Himalayan Crystallines, Bhutan. Journal of Metamorphic Geology 15, 593–612) and are consistent with a more rapid exhumation of deeper levels towards the centre of the High Himalayan Crystalline Complex. Despite the large uncertainties, the *PT* data shown here are also consistent with this interpretation. The apatite fission track results reveal low-temperature cooling and final exhumation of the Main Central Thrust at the same time as in Nepal.

Keywords: Main Central Thrust; Bhutan Himalaya; Metamorphism

1. Introduction

The collision zone between the Indoaustralian and the Asian continental plates forms the largest mountain belt on the earth's surface — the Himalaya. One of the major features associated with this collision is the Main Central Thrust (MCT) which dips to the north and separates the high grade gneisses of the High Himalayan Crystalline Complex (HHC) in the hanging wall, from the greenschist metamorphic rocks of the Lesser Himalaya in the footwall. An inverted metamorphic gradient is associated with this thrust (Gansser, 1964; Le Fort, 1975; Hubbard, 1989; Vannay and Hodges, 1996). The causes of this inversion have been variably interpreted as: (a) the result of post metamorphic inversion of isograds (Brunel and Kienast, 1986); (b) as the result of placing hot rocks in the upper slab onto colder rocks of the lower slab (Le Fort et al., 1986); (c) as the consequence of frictional heating within the MCT itself (Maruo and Kizaki, 1983; Molnar and England, 1990; England and Molnar, 1993); (d) as the consequence of heat focusing (Jaupart and Provost, 1985); (e) as the consequence of folding and shearing of deeper level isotherms during exhumation (Harrison et al., 1997). Recent studies have recognised that an integrated interpretation of the MCT and its inverted gradient must be performed in the context of both the MCT and the second important structure of the Himalaya: the normal South Tibetan Detachment (STD; Burg and Chen, 1984; Burchfield et al., 1992). For example, the model of Grujic et al. (1996) explains the exhumation of the high grade HHC between the reverse MCT and the normal STD with a channel flow model in which the inverted metamorphism is the consequence of the successively more rapid exhumation in the centre of the complex (see also models of Burchfield and Royden, 1985; Harris and Massey, 1994; Avouac and Tapponier, 1993).

* Corresponding author. Tel.: +43-316-380-5682; fax: +43-316-380-9870.

E-mail addresses: kurt.stuewe@kfunigraz.ac.at (K. Stüwe), dfoster@geology.ufl.edu (D. Foster).

1367-9120/01/$ - see front matter
PII: S1367-9120(00)00018-3

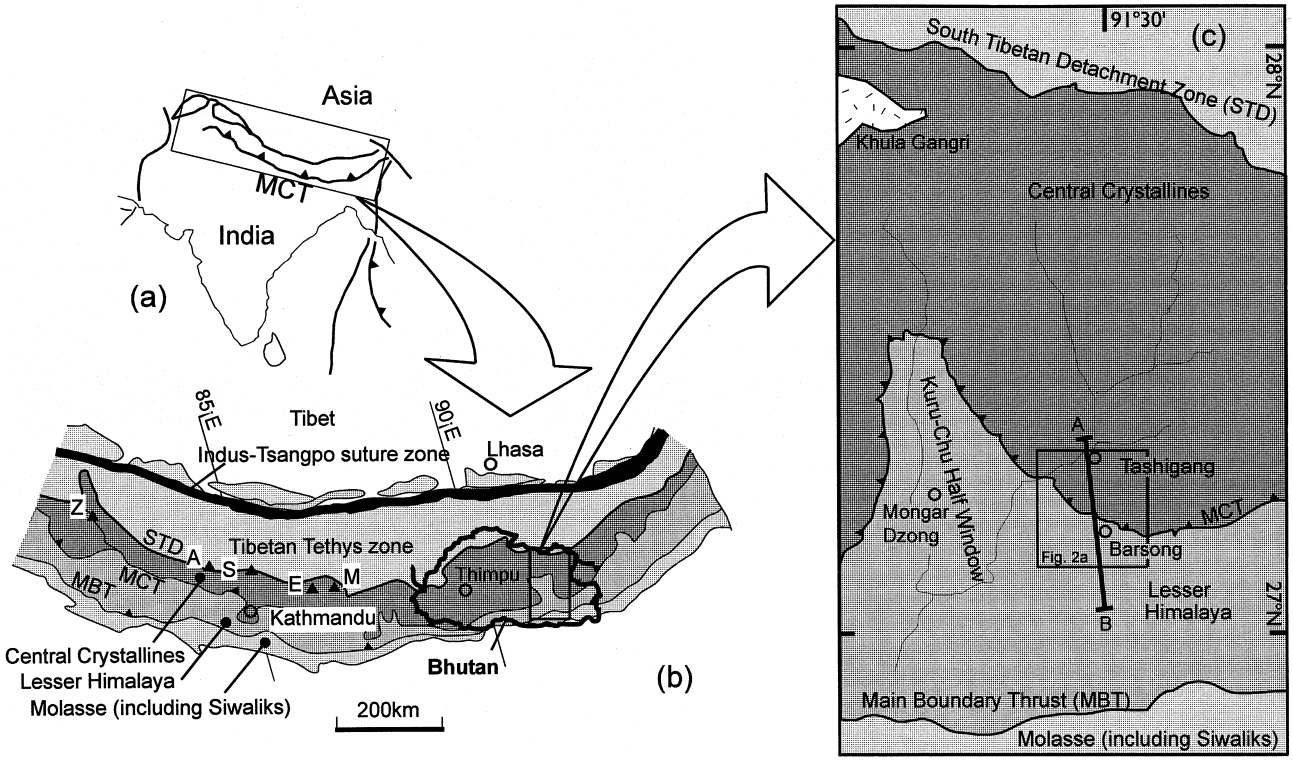

Fig. 1. Location and geological map of the investigated area. (a) The India–Asia collision zone. (b) The central part of the Himalaya with some areas from which radiometric ages are discussed in the text. Z = Zanskar; A = Manaslu; S = Shisha Pangma; E = Everest; M = Makalu. (c) Eastern Bhutan. The profile A–B is shown in Fig. 2(b). The two major roads in the shown area are the road from Thimpu through Mongar Dzong to Tashigang and from Tashigang through Barsong southwards. A small part of the Khula Gangri granite can be seen near the top left. The total pluton is some 50 km in west–east extent. The Ghopu La granite discussed in the text is also northwest of the shown area.

While a consensus on the causes of the apparent inversion of metamorphic isograds has not been reached, a large body of detailed structural and metamorphic data is now emerging in the literature which will assist future interpretations. In particular, this body of data includes several profiles of $^{40}Ar/^{39}Ar$ data across the MCT (Harrison et al., 1997; Hubbard and Harrison, 1989; Copeland et al., 1991); and notably the two-dimensional study of Copeland et al. (2000). It also includes a large range of other age data from the thrust (e.g. Zeitler, 1985) and potentially related plutonic events (e.g. Maluski et al., 1988; Edwards and Harrison, 1997).

However, the large body of data that exists from the region near the western syntaxis of the Himalayan front (for a summary see Searle, 1996) is unmatched by data from the eastern end of the range. This is largely due to the inaccessibility of Bhutan. Data from that region are limited to the original work of Gansser (1983), the outcomes of two Swiss–American expeditions (Davidson et al., 1997; Grujic et al., 1996; Swapp and Hollister, 1991) and few other studies (e.g. Edwards et al., 1996). In this study, we present fission track, $^{40}Ar/^{39}Ar$ and petrological *PT* data from a transect across the MCT in the Bhutan Himalaya that provides an important addition to the dataset of transects across the MCT of the Himalaya.

2. Regional setting and location of transsect

The regional geological setting of the Bhutan Himalaya has been described by Gansser (1983) and its significance in the context of modern Himalayan tectonics is summarised by several recent papers, in particular Davidson et al. (1997; see also: Swapp and Hollister, 1991). In essence, much of Bhutan is dominated by the HHC, which outcrops over a north–south width of about 60–100 km between the STD along the northern border of Bhutan and the MCT [Fig. 1(b)]. In eastern Bhutan, the MCT forms a large half window — the Kuru-Chu half window — exposing the lesser Himalayan rocks to some 50 km further north along the Kuru-Chu valley than along most of the strike length of the MCT [Fig. 1(c)]. The inverted metamorphic gradient associated with the MCT reaches its highest grade within this half window (Gansser, 1983, p. 139). Along the eastern margin of the Kuru-Chu half window, two transects across the MCT are accessible along the roads leaving the township of Tashigang towards the west (towards Thimpu) and towards the south-south-east (towards Barsong; Fig. 1). The former transect has been described by Grujic et al. (1996) and Davidson et al. (1997); the latter transect is some 20 km further east and is described here. Along both transects, the crystalline 'Tashigang unit' of the HHC overlies the

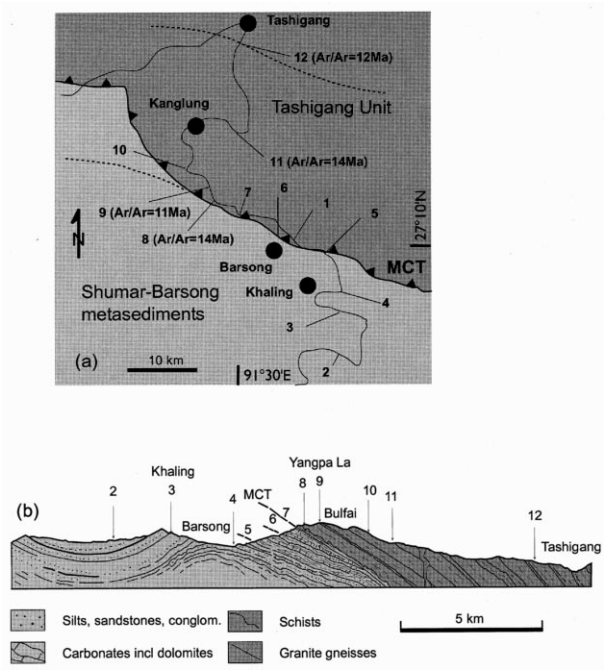

Fig. 2. Sampling locations along the Tashigang transect of the MCT. (a) Part of eastern Bhutan shown in Fig. 1(c). Sample locations are numbered with sample number. For some critical samples the muscovite $^{40}Ar/^{39}Ar$ ages are also shown. The dark shaded area (Tashigang Unit) is part of the Himalayan Crystalline Complex, the light shaded area (Shumar-Barsong metasediments) is part of the Lesser Himalaya. Thin lines are roads. Dashed line south of Tashigang is southern limit of upper amphibolite facies. Dotted line southwest of MCT is southern limit of biotite porphyroblast facies. Isograds are after Gansser (1983). (b) Geological profile shown as profile A–B on Fig. 1(c) (after Gansser, 1983). No vertical exaggeration. Yangpo La is 2500 m above sea level.

'Shumar-Barsong' metasediments of the lesser Himalaya [Fig. 2(a)]. The MCT, separating the two units, dips at an angle of 30–40° to the northwest and is easily defined by the dramatic change of metamorphic grade of the rocks [Fig. 2(b)]. The MCT profile south-south-east of Tashigang is briefly described by Gansser (1983, pp. 64–65). His description, as well as our own observations, suggest that the profile described by Davidson et al. (1997) is very similar to the one described here. At Tashigang, the 'Tashigang unit' is migmatitic with large kyanites in leucosomes. As the MCT is approached, the migmatitic character becomes less apparent, although the structure appears continuous with a north-plunging lineation and a general MCT-parallel dip of the principle schistosity. As the MCT is crossed, rock types include greenschist metamorphic schists and marbles that appear structurally continuous with the hanging wall. Notably, biotite was found in several rocks from the thrust into the footwall that are up to several kilometres from the thrust.

In the investigated profile, 15 samples were collected in varying distances from the MCT (Fig. 2; Table 1). Below, we focus in our discussion on samples 8, 9, 10, 11 and 12. Samples distances from the MCT are quoted as distances perpendicular from our estimate of the location of the MCT.

Table 1
Sample details of this study[a]

Sample number	Lat (km)	Vert (km)	Elev (m)	Location	Rock type/ assemblage
2	71.5	−2.7	2340	S Khaling	quartzvein
3	62	−1.6	2200	S Khaling	greenschist
4	58	−0.8	2040	S Khaling	greenschist
1	48	MCT	2100	N Khaling	greenschist
5	54	MCT	2050	N Khaling	greenschist
6	44	MCT	2150	N Khaling	greenschist
7	41.5	MCT	2200	Landslide	bi-chl-q-cc
8	36	0.2	2540	Yangpho La	gt-bi-mu-q
9	34	0.4	2480	Yangpho La	bi-mu-q-plag
10	28	0.6	2150	4 km S Kangl.	bi-mu-q-plag
11	19	2.1	1750	N Kanglung	bi-mu-q-plag
12	4	4.7	1060	4 km S Tashig.	gt-bi-mu-ky-q

[a] The samples are listed from the footwall to the hanging wall. Negative distances from the MCT are structurally downwards, positive distances structurally upwards.

3. Petrography and mineral chemistry

The studied profile in the region south of Tashigang is largely made up of high grade metapelitic gneisses. Typical assemblages include: garnet–kyanite–biotite–muscovite; garnet–biotite–muscovite; potassium feldspar–biotite–muscovite; kyanite–biotite–muscovite and biotite–muscovite. All assemblages also contain abundant quartz and are fully hydrated. All samples also contain accessory amounts of apatite. Some samples contain accessory tourmaline and sphene. Plagioclase is present occasionally. All samples from the hanging wall of the MCT were investigated in detail with microprobe studies (Table 2). Because of the compositional and structural changes that may be expected with proximity to the MCT, these samples are discussed individually, approaching the MCT.

Sample 12 contains the assemblage garnet–kyanite–biotite–muscovite–quartz and accessory amounts of apatite and tourmaline. Biotite and muscovite define a strong fabric along which the slightly oval-shaped garnets are also aligned. Muscovite growth appears to have outlasted biotite growth. Garnets have inclusion-rich cores and massive rims. Inclusions in garnet are rounded biotite and quartz. Biotite inclusions in garnet are often partially reacted to muscovite. Pressure shadows of biotite and muscovite behind garnets occur. Garnets are slightly zoned with more Fe-rich grain rims than the cores. Their $X_{Fe} = Fe/(Fe + Mn + Mg)$ at the rim is $X_{Fe}^{gt\text{-}rim} = 0.88$ and in the grain cores it is: $X_{Fe}^{gt\text{-}core} = 0.85$. MnO content of garnet is generally less than 1.5 $weight_{\%}$. Biotite and muscovites are compositionally homogeneous with the X_{Fe}^{Bi} ranging only between $0.51 < X_{Fe}^{Bi} < 0.57$. Biotites contain between 0.8 and 1.7% TiO_2, consistently about 0.35% Na_2O and no MnO. The composition of muscovite varies between $0.48 < X_{Fe}^{Mu} < 0.65$. Muscovite also contains no MnO, of the order of 1% TiO_2, and up to 1% Na_2O.

Table 2
Representative microprobe analyses of micas and garnets from the Tashigang traverse across the MCT[a]

Sample:	12.00	12.00	12.00	12.00	11.00	11.00	10.00	10.00	9.00	9.00	8.00	8.00	8.00	8.00
Analysis:	12g4	12g1	12bi3	12mu3	11bbi2	11bmu2	10bi3	10mu3	9abi7	9amu1	8g4 m	8g2rim	8bi7	8mu13
Mineral	gcore	grim	bi	mu	bi	mu	bi	mu	bi	mu	gcore	grim	bi	mu
SiO_2	37.89	37.54	35.72	46.51	35.78	45.75	36.95	46.48	36.80	46.61	36.92	38.33	36.19	45.63
TiO_2	0.03	0.03	2.12	0.86	2.68	1.34	2.63	1.10	2.49	1.78	0.04	–	2.22	1.24
Al_2O_3	21.69	20.84	19.07	34.69	17.50	32.18	17.34	32.39	17.38	32.42	20.87	21.33	18.61	31.12
MgO	4.15	2.67	9.92	0.85	11.98	1.86	11.37	1.70	12.34	1.75	1.51	2.93	8.82	1.63
CaO	2.35	1.69	0.00	0.00	0.02	0.05	0.01	0.06	0.01	0.00	3.62	6.91	0.01	0.01
MnO	1.22	1.54	0.05	0.06	0.15	0.05	0.22	0.00	0.24	0.18	6.66	0.75	0.09	0.03
FeO[b]	34.94	36.90	19.99	1.58	17.42	1.72	18.33	1.66	16.42	2.03	30.49	30.66	22.33	2.04
Na_2O	–	–	0.31	0.89	0.10	0.32	0.12	0.29	0.12	0.25	–	–	0.14	0.54
K_2O	–	–	8.77	8.92	9.41	9.85	9.39	9.55	9.42	11.94	–	–	9.06	13.40
Total	102.28	101.20	95.95	94.36	95.04	93.11	96.35	93.24	95.21	96.97	100.10	100.91	97.47	95.62
Oxygens	12.00	12.00	11.00	11.00	11.00	11.00	11.00	11.00	11.00	11.00	12.00	12.00	11.00	11.00
Si	2.96	3.00	2.70	3.10	2.71	3.11	2.76	3.15	2.76	3.10	2.99	3.02	2.72	3.11
Ti	0.00	0.00	0.12	0.04	0.15	0.07	0.15	0.06	0.14	0.09	0.00	–	0.13	0.06
Al	2.00	1.96	1.70	2.73	1.56	2.58	1.53	2.58	1.54	2.54	1.99	1.98	1.65	2.50
Mg	0.48	0.32	1.12	0.09	1.35	0.19	1.27	0.17	1.38	0.17	0.18	0.34	0.99	0.17
Ca	0.20	0.15	0.00	0.00	0.00	0.00	0.00	0.00	0.00	0.00	0.31	0.58	0.00	0.00
Mn	0.08	0.10	0.00	0.00	0.01	0.00	0.01	0.00	0.02	0.01	0.46	0.05	0.01	0.00
Fe	2.20	2.44	1.26	0.08	1.10	0.05	1.15	0.05	1.03	0.11	2.04	2.02	1.40	0.12
Na	–	–	0.05	0.12	0.02	0.04	0.02	0.04	0.02	0.03	–	–	0.02	0.07
K	–	–	0.85	1.76	0.91	0.86	0.90	0.83	0.90	1.01	–	–	0.87	1.17
Total	7.92	7.97	7.78	6.92	7.82	6.90	7.78	6.85	7.79	7.07	7.97	7.99	7.78	7.20

[a] Recalculated mineral formulae were calculated with the software ax of Holland (unpublished software).
[b] FeO measured as total Fe.

Table 3
Some examples of average pressure temperature calculations for samples 10 and 12[a]

Average *PT* calculated for sample 12 (g-bi-mu-ky-q assemblage)

End-members:	py	alm	phl	ann	east	mu	cel	ky	q	H_2O
Activities (a):	0.005	0.378	0.0404	0.0585	0.0429	0.668	0.0379	1.00	1.00	1.00
$\sigma(\ln a)$:	0.61852	0.15000	0.38304	0.33687	0.37719	0.10000	0.38912	0	0	0
Independent reactions			$P(T)$	$\sigma(P)$	a	S.D. (a)	b	c	ln K	S.D. (ln K)
(1) 3east + 6q = py + phl + 2mu			10.6	3.94	28.60	7.58	0.00451	−3.157	0.132	1.360
(2) phl + east + 6q = py + 2cel			12.8	4.44	72.58	11.30	0.00850	−3.148	−5.486	1.130
(3) py + 3east + 4q = 3phl + 4ky			9.1	7.49	−80.97	7.62	0.07048	−1.959	5.118	1.727
(4) alm + 3east + 6q = 2py + ann + 2mu			14.0	5.11	75.14	7.60	−0.00851	−2.870	−3.823	1.728
Average pressure and temperature:										
T = 647°C, S.D. = 152,										
P = 6.5 kbar, S.D. = 3.7, cor = −0.169, f = 1.50										

Average T calculated for sample 10 (bi-mu-ksp assemblage)

End-members:		phl	east	mu	cel	q	ksp	H_2O
Activities (a):		0.0643	0.0375	0.603	0.0800	1.00	1.00	1.00
$\sigma(\ln a)$:		0.33429	0.39012	0.10000	0.30859	0	0	0
Independent reactions — calculations at P = 9.5 kbar [for $x(H_2O) = 1.0$]	$T(P)$	S.D. (T)	a	S.D. (a)	b	c	ln K	S.D. (ln K)
(1) east + cel = phl + mu	870	3983	−21.99	6.03	−0.00199	−0.005	2.559	0.608
(2) 3cel = phl + 3q + 2ksp + $2H_2O$	634	131	50.52	16.74	−0.14305	4.439	4.833	0.984
Average temperatures [for $x(H_2O) = 1.0$]								
	P	4.0	6.0	8.0	10.0	12.0	14.0	16.0
	av T	539	595	654	713	773	834	895
	$\sigma(T)$	68	69	73	76	81	85	90
	f	0.8	0.7	0.5	0.4	0.2	0.1	0.1

[a] Mineral abbreviations are those used in THERMOCALC of Powell and Holland (1988).

Samples 11, 10 and 9 consist of the paragenesis biotite–muscovite–quartz. Plagioclase and K-feldspar occur as well. Apatite is an abundant accessoric phase. Biotite and muscovite define a strong schistosity and lineation. Biotites and muscovites have generally lower X_{Fe} than the garnet-bearing samples 12 and 8. In all three samples biotite has a fairly constant composition ($0.42 < X_{Fe}^{Bi} < 0.48$). Muscovite composition varies more ($0.2 < X_{Fe}^{Mu} < 0.4$). Sample 8 contains the assemblage garnet–biotite–muscovite–quartz. However, in contrast to sample 12, garnets are inclusion-poor and form idiomorphic porphyroblasts several millimetres in size. Grains of all sizes are zoned with slightly more Fe-rich cores than the rims, but larger grains appear to have more pronounced zoning profiles than smaller grains. X_{Fe} varies between $X_{Fe}^{gt\text{-}core} = 0.76$ and $X_{Fe}^{gt\text{-}rim} = 0.83$. Manganese contents are also strongly zoned with up to 6 weight% in the core of grains that are practically Mn-free at the rim. Micas are Fe-richer than in the garnet-free samples with similar X_{Fe} as in sample 12. Typical values are around: $X_{Fe}^{Mu} = 0.41$ and $X_{Fe}^{Bi} = 0.58$. As in all other samples, the micas define a strong fabric.

4. Pressure and temperature estimates

The assemblages discussed above are stable over a wide range of pressures and temperatures. Petrogenetic grids are therefore of limited use for constraining the conditions of crystallisation. Average temperature and average pressure–temperature calculations were therefore performed using the computer software THERMOCALC of Powell and Holland (1988) with the thermodynamic dataset of Holland and Powell (1990). All parageneses described above can be described in the system K_2O–FeO–MgO–Al_2O_3–SiO_2–H_2O (KFMASH). In this system, the assemblage of sample 12 is thermodynamically divariant, but up to 10 end-member activities can be derived so that up to four independent reactions are available for average *PT* calculations. The other assemblages are thermodynamically tri- or quadrivariant and therefore some of the results discussed below have quite large error bars.

Average *PT* estimates for sample 12 were performed with garnet core and garnet rim equilibria. *PT* estimates depend on the choice of end-members used for the calculations. Using the full KFMASH assemblage, that is using end-member activities of almandine and pyrope for garnet, of annite, phlogopite and eastonite for biotite and of muscovite and celadonite for white mica as well as kyanite, quartz and H_2O give temperatures between 610 ± 120 and 650 ± 150°C at pressure estimates that are consistently around 6.5 ± 3 kbar for core compositions of garnet (Table 3). Excluding the eastonite end member from the calculations results in 30–50°C higher temperatures and lower pressures around 4–5 kbar. However, these calculations have very large uncertainties on P estimates and bad fit parameters. Calculations in KMASH (that is, excluding the annite and almandine end-member from the calculation) on the other hand, improves the fit and gives in all calculations

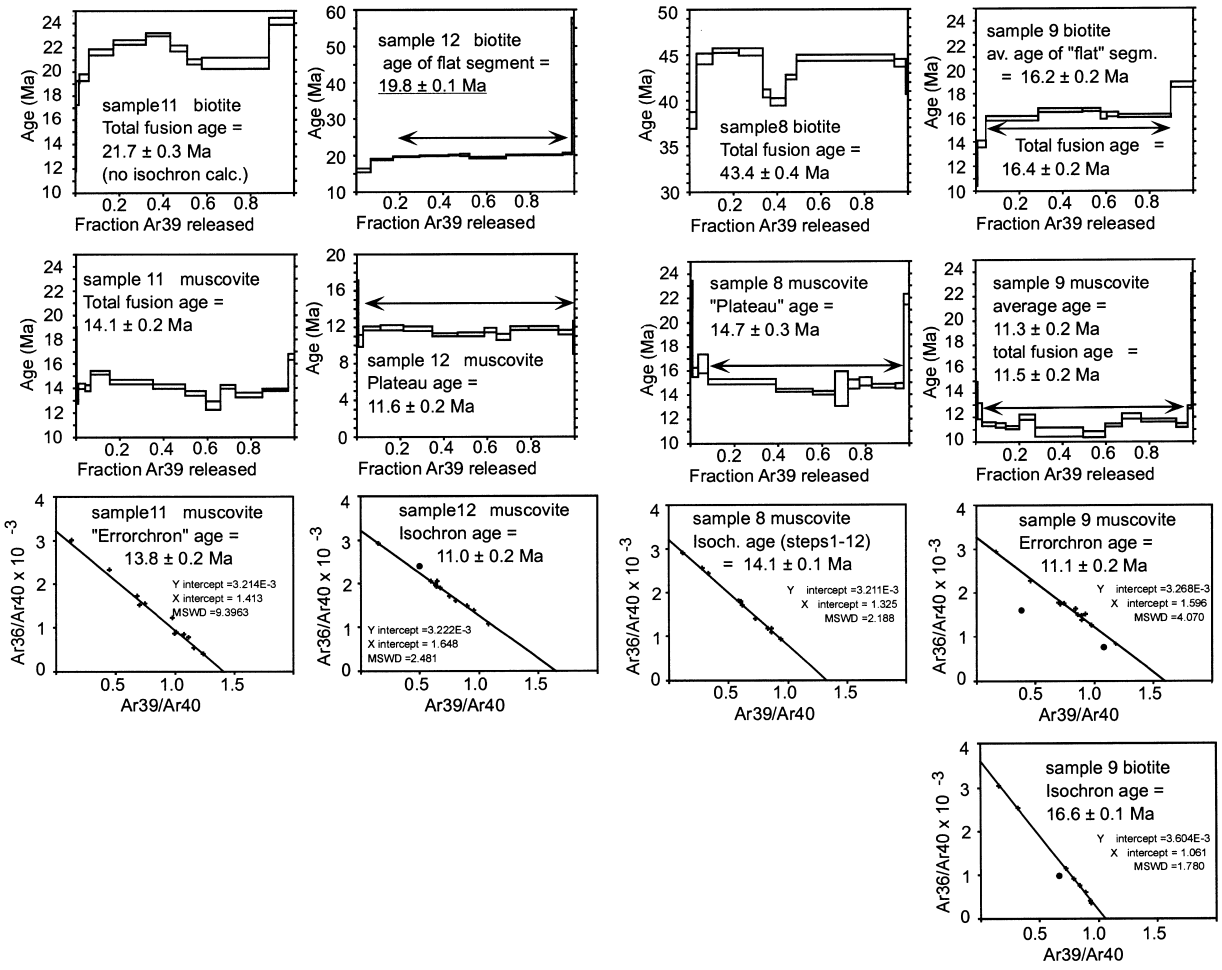

Fig. 3. $^{40}Ar/^{39}Ar$ age spectra and inverse isochron plots for muscovite and biotite from samples 8, 9, 11 and 12.

about 20°C lower temperatures but substantially higher pressures around 10 and 11 ± 3 kbar than in the KFMASH calculations. Using rim compositions of garnet gives about 510–550°C ± 100°C. Pressure estimates are similar to those of the calculations using garnet cores. The changes of these estimates that occur due to the exclusion of annite or eastonite end members from the full system calculations correspond to those discussed above. Average-*T* and average-*P* calculations performed on the same assemblage confirm the results of the average *PT* calculations.

The equilibria between biotite and muscovite are largely temperature dependent and are therefore of limited use to constrain formation pressures. For an assumed pressure of 4 kbar, samples 8, 9, 10 and 11 give formation temperatures of 496, 539, 539 and 545°C, respectively. All temperatures increase by about 60°C for every kbar higher assumed pressure. An example from sample 10 is shown in Table 3. Despite the large uncertainties associated with the absolute temperature estimates, the relative changes of temperature may be of some significance (Powell, personal communication, 1998). These data indicate a slight increase in temperature at larger distances from the thrust.

5. $^{40}Ar/^{39}Ar$ results

5.1. Analytical technique

Muscovite and biotite were analysed from four samples at La Trobe University, Australia following the methods summarised in Foster et al. (1999). Argon gas from all samples was extracted using the furnace method on hand picked mineral separates of about 5 mg. Age spectra are shown in Fig. 3(a,b) and the isotopic results from release steps are given in Table 4. The muscovite and biotite apparent ages (total fusion, isochron and/or plateau) range from 14.7 to 11.0 and 43.4 to 16.6 Ma.

5.2. Results

5.2.1. Sample 8

Muscovite from sample 8 gave a slightly discordant age spectrum with an average age of 14.7 ± 0.2 Ma for steps 3–12. Steps 1–12 of this sample fall on a well defined isochron with an age of 14.1 ± 0.1 Ma, which is interpreted to give the bulk cooling age of this

Table 4
$^{40}Ar/^{39}Ar$ data

Temperature (°C)	^{36}Ar (mol)	^{37}Ar (mol)	^{39}Ar (mol)	^{40}Ar (mol)	$^{40}Ar^{a}$	$^{40}Ar^{a}/^{39}ArK$	Cum.^{39}Ar (%)	Calc.age (Ma)	Error (Ma)	Ca/K (±1 S.D.)
8 biotite, $J = 0.010286$										
600	1.38*E*-15	9.13*E*-15	1.45*E*-13	7.08*E*-13	42.1	2.058	3.31	37.8	0.92	1.20*E*-01
650	6.26*E*-16	1.21*E*-14	3.18*E*-13	9.62*E*-13	80.4	2.432	10.59	44.57	0.58	7.21*E*-02
700	3.78*E*-16	3.05*E*-14	5.16*E*-13	1.40*E*-12	91.7	2.485	22.4	45.53	0.25	1.12*E*-01
750	2.50*E*-16	2.84*E*- 14	4.74*E*-13	1.25*E*- 12	93.8	2.474	33.25	45.34	0.41	1.14*E*-01
800	1.48*E*-16	9.73*E*-15	1.62*E*-13	4.05*E*-13	88.8	2.223	36.96	40.78	0.43	1.14*E*-01
900	1.96*E*-16	2.21*E*-14	3.09*E*-13	7.30*E*-13	91.8	2.169	44.02	39.81	0.44	1.36*E*-01
950	1.28*E*-16	1.41*E*- 14	2.13*E*- 13	5.33*E*-13	92.6	2.322	48.88	42.58	0.25	1.26*E*-01
1050	6.83*E*-16	1.10*E*-13	1.96*E*-12	4.98*E*- 12	95.6	2.436	93.64	44.65	0.33	1.07*E*-01
1100	1.13*E*-16	1.43*E*-14	2.24*E*-13	5.75*E*- 13	93.9	2.406	98.77	44.1	0.41	1.21*E*-01
1450	5.01*E*-16	1.23*E*-14	5.37*E*-14	2.70*E*-13	45.3	2.277	100	41.77	1.1	4.36*E*-01
Total	4.41*E*-15	2.63*E*-13	4.37*E*-12	1.18*E*-11		2.397		43.95	0.39	
8 muscovite, $J = 0.010415$										
600	5.66*E*-16	4.55*E*-15	2.24*E*-14	1.94*E*-13	13.9	1.202	1.03	22.45	1	3.87*E*-01
700	4.27*E*-16	3.49*E*-15	5.70*E*-14	1.75*E*-13	27.6	0.848	3.67	15.86	0.37	1.16*E*-01
750	8.86*E*-16	4.21*E*-15	9.56*E*-14	3.48*E*-13	24.4	0.887	8.08	16.59	0.77	8.37*E*- 02
800	1.30*E*-15	2.43*E*-14	6.71*E*-13	9.33*E*- 13	58	0.807	39.06	15.1	0.21	6.90*E*-02
825	3.61*E*-16	1.16*E*-14	3.59*E*- 13	3.87*E*-13	71.3	0.769	55.63	14.39	0.12	6.17*E*-02
860	3.10*E*- 16	9.96*E*- 15	2.25*E*- 13	2.64*E*- 13	64.4	0.756	66.02	14.15	0.14	8.41*E*-02
950	3.82*E*-16	3.43*E*-15	1.27*E*-13	2.13*E*-13	46.1	0.775	71.86	14.5	1.43	5.16*E*-02
1000	3.55*E*-16	3.66*E*-15	1.13*E*-13	1.96*E*-13	45.7	0.795	77.07	14.87	0.37	6.17*E*-02
1050	3.43*E*-16	2.21*E*-15	1.23*E*-13	2.02*E*-13	49	0.806	82.75	15.08	0.33	3.41*E*-02
1100	3.43*E*-16	8.69*E*-15	2.39*E*-13	2.92*E*-13	64.4	0.786	93.79	14.72	0.17	6.91*E*−02
1150	1.03*E*-16	4.58*E*-15	7.95*E*-14	9.37*E*-14	66.7	0.787	97.46	14.72	0.19	1.10*E*-01
1450	3.43*E*-16	4.14*E*-15	5.51*E*-14	1.66*E*-13	38.8	1.171	100	21.87	0.41	1.43*E*-01
Total	5.72*E*-15	8.49*E*-14	2.17*E*-12	3.46*E*-12		0.808		15.12	0.31	
9 biotite, $J = 0.0097994$										
500	5.21*E*-16	1.93*E*-15	2.69*E*-14	1.71*E*-13	9.9	0.633	0.71	11.16	0.71	1.36*E*-01
600	1.18*E*-15	9.90*E*-15	1.46*E*-13	4.64*E*-13	24.8	0.786	4.59	13.84	0.31	1.29*E*-01
700	1.48*E*-15	3.13*E*-14	9.18*E*-13	1.28*E*-12	64.9	0.905	28.94	15.93	0.19	6.49*E*-02
750	3.47*E*-16	1.52*E*-14	7.57*E*-13	8.27*E*-13	86.4	0.943	49.02	16.6	0.15	3.81*E*-02
800	1.26*E*-16	3.84*E*-15	3.17*E*-13	3.41*E*-13	87.8	0.946	57.42	16.65	0.12	2.30*E*-02
850	1.05*E*-16	1.50*E*-15	1.14*E*-13	1.37*E*-13	76.3	0.919	60.44	16.17	0.28	2.51*E*-02
950	2.39*E*-16	4.99*E*-15	2.01*E*-13	2.59*E*-13	71.8	0.923	65.77	16.24	0.18	4.72*E*-02
1050	6.25*E*-16	2.31*E*-14	9.02*E*-13	1.02*E*-12	80.8	0.916	89.69	16.13	0.13	4.87*E*-02
1450	5.84*E*-16	1.53*E*-14	3.89*E*-13	5.90*E*-13	70	1.063	100	18.7	0.23	7.46*E*-02
Total	5.21*E*-15	1.07*E*-13	3.77*E*-12	5.09*E*-12		0.93		16.37	0.18	
9 muscovite, $J = 0.0099167$										
550	7.60*E*-16	2.30*E*-15	4.39*E*-14	2.59*E*-13	13.1	0.775	0.78	13.81	1.14	9.94*E*-02
650	6.17*E*-16	6.87*E*-15	1.24*E*-13	2.70*E*-13	32.1	0.703	2.96	12.53	0.67	1.06*E*-01
750	6.19*E*-16	1.43*E*-14	3.50*E*-13	4.12*E*-13	54.7	0.644	9.15	11.49	0.16	7.75*E*-02
780	3.44*E*-16	7.76*E*-15	2.63*E*-13	2.73*E*-13	61.6	0.639	13.8	11.4	0.19	5.60*E*-02
810	5.72*E*-16	1.73*E*-14	3.41*E*-13	3.86*E*-13	55.4	0.627	19.84	11.19	0.14	9.66*E*-02
840	1.08*E*-15	1.65*E*-14	4.20*E*-13	6.08*E*-13	46.5	0.674	27.26	12.03	0.19	7.49*E*-02
900	2.48*E*-15	6.64*E*-14	1.25*E*-12	1.50*E*-12	50.5	0.606	49.45	10.82	0.39	1.01*E*-01
950	9.69*E*-16	1.58*E*-14	5.84*E*-13	6.42*E*-13	54.3	0.596	59.79	10.63	0.25	5.14*E*-02
1000	1.00*E*-15	1.21*E*-14	4.20*E*-13	5.69*E*-13	47.1	0.638	67.22	11.39	0.14	5.49*E*-02
1050	1.22*E*-15	1.88*E*-14	4.96*E*-13	7.02*E*-13	47.8	0.677	75.99	12.07	0.23	7.20*E*-02
1100	1.45*E*-15	2.91*E*-14	9.24*E*-13	1.05*E*-12	58.1	0.659	92.35	11.75	0.12	5.99*E*-02
1150	2.17*E*-16	2.19*E*-14	2.97*E*-13	2.55*E*-13	74	0.637	97.61	11.36	0.16	1.40*E*-01
1200	6.89*E*-17	6.19*E*-15	9.49*E*-14	8.92*E*-14	76.3	0.717	99.29	12.79	0.13	1.24*E*-01
1450	1.72*E*-16	3.80*E*-15	4.03*E*-14	1.06*E*-13	51.9	1.366	100	24.27	0.42	1.79*E*-01
Total	1.16*E*-14	2.39*E*-13	5.65*E*-12	7.12*E*-12		0.645		11.5	0.24	
11 biotite, $J = 0.010684$										
500	4.04*E*-16	2.15*E*-15	1.47*E*-14	1.29*E*-13	7.7	0.674	0.36	12.94	1.13	2.78*E*-01
600	6.49*E*-16	3.00*E*-15	5.31*E*-14	2.42*E*-13	20.6	0.941	1.65	18.05	0.99	1.08*E*-01
650	6.82*E*-16	1.11*E*-14	1.77*E*-13	3.83*E*-13	47	1.019	5.95	19.53	0.27	1.19*E*-01
700	4.23*E*-16	1.87*E*-14	4.57*E*-13	6.46*E*-13	79.9	1.129	17.07	21.63	0.27	7.79*E*-02
750	1.96*E*-16	2.08*E*-14	6.17*E*-13	7.88*E*-13	91.7	1.172	32.07	22.45	0.18	6.41*E*-02
850	1.87*E*-16	1.48*E*-14	4.62*E*-13	6.17*E*-13	90.2	1.204	43.31	23.06	0.13	6.09*E*-02
950	1.71*E*-16	1.12*E*-14	3.05*E*-13	4.03*E*-13	86.6	1.145	50.73	21.94	0.24	6.99*E*-02

Table 4 (*continued*)

Temperature (°C)	^{36}Ar (mol)	^{37}Ar (mol)	^{39}Ar (mol)	^{40}Ar (mol)	^{40}Ar[a]	^{40}Ar[a]/^{39}ArK	Cum.^{39}Ar (%)	Calc.age (Ma)	Error (Ma)	Ca/K (±1 S.D.)
1000	1.67*E*-16	1.36*E*-14	2.78*E*-13	3.55*E*-13	85.3	1.088	57.49	20.86	0.22	9.29*E*-02
1100	6.04*E*-16	6.15*E*-14	1.28*E*-12	1.57*E*-12	87.8	1.08	88.5	20.7	0.48	9.16*E*-02
1450	8.85*E*-16	2.81*E*-14	4.73*E*-13	8.61*E*-13	69.2	1.26	100	24.13	0.29	1.13*E*-01
Total	4.37*E*-15	1.85*E*-13	4.11*E*-12	5.99*E*-12		1.134		21.72	0.31	
11 muscovite, $J = 0.010824$										
550	2.94*E*-16	6.73*E*-15	1.23*E*-14	9.70*E*-14	11	0.862	0.31	16.75	2.34	1.04*E* + 00
650	1.85*E*-16	2.44*E*-15	3.50*E*-14	7.91*E*-14	30.7	0.695	1.19	13.52	0.76	1.33*E*-01
750	2.43*E*-16	5.85*E*-15	1.15*E*-13	1.57*E*-13	53.5	0.728	4.1	14.15	0.24	9.66*E*-02
780	2.68*E*-16	6.06*E*-15	1.05*E*-13	1.55*E*-13	48.5	0.719	6.74	13.99	0.26	1.10*E*-01
820	7.47*E*-16	1.91*E*-14	3.42*E*-13	4.92*E*-13	54.5	0.785	15.37	15.27	0.16	1.06*E*-01
860	6.93*E*-16	3.20*E*-14	7.78*E*-13	7.94*E*-13	73.2	0.747	35.02	14.52	0.19	7.82*E*-02
900	2.78*E*-16	1.72*E*-14	5.91*E*-13	5.18*E*-13	82.7	0.726	49.93	14.11	0.18	5.53*E*-02
950	2.97*E*-16	1.80*E*-14	3.65*E*-13	3.46*E*-13	73.6	0.697	59.14	13.57	0.2	9.40*E*-02
1000	3.44*E*-16	1.22*E*-14	2.69*E*-13	2.79*E*-13	62.5	0.648	65.94	12.61	0.35	8.60*E*-02
1050	2.54*E*-16	1.14*E*-14	2.80*E*-13	2.81*E*-13	72.2	0.725	73.01	14.1	0.14	7.73*E*-02
1100	3.54*E*-16	1.89*E*-14	4.91*E*-13	4.49*E*-13	75.5	0.691	85.4	13.44	0.21	7.32*E*-02
1150	1.57*E*-16	1.47*E*-14	4.62*E*-13	3.81*E*-13	86.4	0.711	97.08	13.84	0.08	6.04*E*-02
1450	1.08*E*-16	9.73*E*-15	1.16*E*-13	1.31*E*-13	75.2	0.852	100	16.56	0.24	1.60*E*-01
Total	4.22*E*-15	1.74*E*-13	3.96*E*-12	4.16*E*-12		0.725		14.1	0.2	
12 biotite, $J = 0.010160$										
600	1.47*E*-15	9.46*E*-15	2.65*E*-13	6.70*E*-13	34.6	0.876	6.75	15.98	0.51	6.79*E*-02
650	4.52*E*-16	1.05*E*-14	3.91*E*-13	5.45*E*-13	74.6	1.04	16.72	18.97	0.14	5.08*E*-02
700	2.81*E*-16	1.31*E*-14	4.87*E*-13	6.14*E*-13	85.5	1.078	29.12	19.65	0.15	5.12*E*-02
750	1.97*E*-16	1.16*E*-14	5.24*E*-13	6.36*E*-13	89.8	1.088	42.49	19.84	0.09	4.22*E*-02
800	9.84*E*-17	3.99*E*-15	1.99*E*-13	2.50*E*-13	87.3	1.099	47.56	20.03	0.13	3.82*E*-02
900	1.62*E*-16	9.17*E*-15	1.76*E*-13	2.43*E*-13	79.7	1.1	52.05	20.05	0.27	9.90*E*-02
1000	3.53*E*-16	2.25*E*-14	6.62*E*-13	8.15*E*-13	86.3	1.061	68.94	19.35	0.19	6.46*E*-02
1050	1.80*E*-16	1.50*E*-14	5.58*E*-13	6.75*E*-13	91.1	1.102	83.16	20.09	0.18	5.11*E*-02
1100	1.31*E*-16	1.33*E*-14	4.55*E*-13	5.45*E*-13	91.9	1.1	94.76	20.05	0.09	5.56*E*-02
1150	6.81*E*-17	8.22*E*-15	1.67*E*-13	2.09*E*-13	89.6	1.119	99.03	20.39	0.16	9.34*E*-02
1450	5.48*E*-16	7.89*E*-15	3.81*E*-14	2.82*E*-13	42.7	3.157	100	56.96	0.77	3.93*E*-01
Total	3.94*E*-15	1.25*E*-13	3.92*E*-12	5.48*E*-12		1.089		19.85	0.18	
12 muscovite, $J = 0.01003$										
550	5.87*E*-16	4.82*E*-15	3.02*E*-14	2.01*E*-13	13.6	0.906	0.68	16.33	0.84	3.04*E*-01
650	4.73*E*-16	2.38*E*-14	9.57*E*-14	1.94*E*-13	28.7	0.583	2.82	10.53	0.66	4.72*E*-01
0	1.24*E*-15	2.03*E*-14	3.54*E*-13	6.03*E*-13	38.5	0.656	10.76	11.84	0.21	1.09*E*-01
780	1.46*E*-15	1.70*E*-14	4.83*E*-13	7.58*E*-13	42.3	0.664	21.57	11.98	0.3	6.67*E*-02
810	1.17*E*-15	1.75*E*-14	5.82*E*-13	7.33*E*-13	52	0.655	34.59	11.82	0.24	5.73*E*-02
840	7.64*E*-16	1.91*E*-14	5.25*E*-13	5.57*E*-13	58.4	0.618	46.36	11.16	0.16	6.89*E*-02
900	9.13*E*-16	2.46*E*-14	5.42*E*-13	6.13*E*-13	55.1	0.622	58.51	11.23	0.19	8.61*E*-02
950	7.23*E*-16	8.60*E*-15	2.53*E*-13	3.81*E*-13	43.1	0.647	64.19	11.67	0.23	6.45*E*-02
1000	9.13*E*-16	1.43*E*-14	2.83*E*-13	4.44*E*-13	38.6	0.605	70.54	10.93	0.32	9.59*E*-02
1050	1.17*E*-15	1.22*E*-14	3.76*E*-13	5.97*E*-13	41.4	0.658	78.96	11.87	0.21	6.17*E*-02
1100	1.39*E*-15	1.86*E*-14	6.08*E*-13	8.19*E*-13	49	0.66	92.58	11.91	0.21	5.82*E*-02
1150	2.99*E*-16	1.55*E*-14	2.98*E*-13	2.80*E*-13	67.4	0.632	99.26	11.41	0.23	9.89*E*-02
1450	2.66*E*-16	3.11*E*-15	3.30*E*-14	9.84*E*-14	20.1	0.6	100	10.83	1.84	1.79*E*-01
Total	1.14*E*-14	2.00*E*-13	4.46*E*-12	6.28*E*-12		0.643		11.61	0.25	

[a] ^{40}Ar decay constant = 5.543*E*-10 correction factors $^{36/37}$Ar = 3.50*E*-4, $^{39/37}$Ar = 7.86*E*-4, ^{40}Ar/^{39}Ar = 2.7*E*-2.

muscovite. Biotite from sample 8 gave a discordant spectrum with maximum and minimum ages of about 38 and 46 Ma, and a total fusion age of 43.4 ± 0.4 Ma. The data from this biotite fail to define an isochron for significant fraction of the gas, suggesting mixing of more than two gas reservoirs.

5.2.2. Sample 9

The age spectrum obtained for muscovite from sample 9 is mildly U-shaped with an average age of 11.3 ± 0.2 Ma for steps 3–12, which are nearly concordant. Isochron analysis of steps 1–12 gives an age of 11.1 ± 0.2 Ma with a slightly elevated MSWD of 4. We interpret the isochron age to be the best estimate of the cooling age for the muscovite. Biotite from sample 8 gave an age gradient from about 11–19 Ma, with a plateau-like segment at 16.2 ± 0.2 Ma. Steps 1–12 define a linear array on an isochron plot, however, the stair–step age gradient violates the assumption that the sample has a single radiogenic Ar component, which suggests that the alignment is accidental.

5.2.3. Sample 11

Muscovite from sample 11 gave a relatively flat but slightly discordant age spectrum with a total fusion age of 14.1 ± 0.2 Ma. The isochron for this sample reveals excess scatter and an 'errorchron' age of 13.8 ± 0.2 Ma. Biotite from sample 11 gave a discordant spectrum with an age gradient from about 18–24 Ma with a distinctive hump shape in the mid-release steps. The form of this age spectrum suggests the presence of excess argon.

5.2.4. Sample 12

The Ar–Ar results from sample 12 are similar to those of sample 9. The muscovite gave plateau and isochron ages of 11.6 ± 0.2 and 11.0 ± 0.2 Ma, respectively. We consider the isochron age the best estimate of the cooling age for the muscovite. Biotite from sample 12 gave a discordant spectrum with an age gradient from ~16 to 20 Ma. The average age of the central part of this age spectrum is 19.8 ± 0.1 Ma, which may have no geological significance in terms of cooling.

5.3. Interpretation of Ar–Ar results

For all four samples the biotite and muscovite Ar–Ar apparent ages are reverse discordant such that the muscovite ages are distinctly younger than the biotite ages. This relationship is unusual because the argon retentivity in muscovite is generally considerably greater than for biotite, giving muscovite a higher closure temperature for simple cooling situations (McDougall and Harrison, 1988). However, this relationship is seen in several studies of Himalayan micas. The reverse discordance is most likely caused by the presence of excess ^{40}Ar in the biotites, as is suggested by the form of at least two of the biotite age spectra. Excess argon in biotite does not always produce diagnostic age spectra because of hydrous breakdown during vacuum extraction (Roddick et al., 1980). Copeland et al. (1991, 2000) found significant excess argon in biotite from within and above the MCT zone in Nepal so it is not unexpected that a similar problem arises with these data. The source of the excess argon is probably from the flow of fluids within the MCT zone that are charged with ^{40}Ar from deeper structural levels. Muscovite has a much lower solubility for argon than biotite, which explains why they are not strongly effected by excess argon and the isochrons give geologically significant results.

The only other reasonable explanation for reverse discordance in these data would be if muscovite growth significantly outlasted biotite growth. However, for this to be correct all of the muscovite would have to have grown/recrystallised at temperatures less than about 320°C or very quickly in order to not have reset the biotite K–Ar system. The mineral paragenesis and compositional data suggest this is unlikely, and that the biotite dates should be treated as anomalous due to the variable concentrations of excess argon.

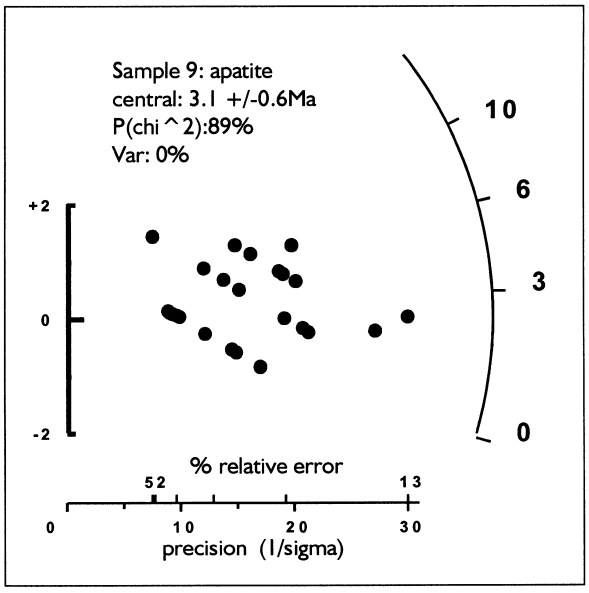

Fig. 4. Radial plot of the apatite fission track results from sample 9 showing the distribution of measured single grain ages. The single grain ages are plotted along radial projections from the origin to the curved age axis with the relatively more precise measurements falling furthest to the right.

The muscovite cooling ages effectively place a minimum age for the amphibolite facies metamorphism of the central metamorphic zone. They either record rapid cooling events at ca. 14 and 11 Ma for separate parts of the sequence or the exhumation of an argon partial retention zone (Foster and John, 1999; John and Foster, 1993) at or after ca. 11 Ma. In the second case, the ca. 11 Ma samples would have been from a slightly deeper structural level than the ca. 14 Ma samples. In either case, the coincidence of the two pairs of ca. 11 and 14 Ma ages strongly suggest repetition/stacking of rock packages within the thrust zone and cooling to below about 400–350°C (approximate range of muscovite closure temperatures: e.g. McDougall and Harrison, 1988; Kirchner et al., 1996). Telescoping in the thrust zone post-dated 11 Ma and may have occurred during ramping on the MCT as suggested by Harrison et al. (1997) for a similar sequence along strike in Nepal.

6. Apatite fission track results

The apatite fission track analysis followed methods summarised in Foster and Gleadow (1996). Analysis of 24 grains from sample 9 gave a pooled age of 3.1 ± 0.6 Ma (Fig. 4). This was derived from a counted standard track density of 1.30 (4000) 10^4 cm^{-2}, fossil track density of 1.628 (28) 10^4 cm^{-2}, induced track density of 1.177 (1808) 10^6 cm^{-2}, uranium content of 11.3 ppm and a chi square probability$_{\%}$ of 89.4. The low spontaneous track density associated with the young fission track age did not provide enough confined tracks to measure a population of track lengths. However, the ca. 3 Ma age defines the cooling

of the MCT through 110–60°C (Gleadow and Duddy, 1981). A larger number of apatite fission track ages from above and below the MCT near Kathmandu also give cooling ages of about 3 Ma (Copeland et al., 2000).

7. Discussion

The age data presented above must be interpreted in the context of other available age data from the region. In the Tashigang region, Gansser (1983) reported of a 26 Ma Rb–Sr muscovite age, which is older than any of the $^{40}Ar/^{39}Ar$ ages discussed here and might indicate very slow cooling. However, a range of other ages obtained by Gansser (1983) from other locations in Bhutan all give Rb–Sr mica ages between 9 and 13 Ma. The Khula Kangri granite, some 80 km northwest of Tashigang has a crystallisation age of 12.5 ± 0.4 Ma (Edwards and Harrison, 1997) and a $^{40}Ar/^{39}Ar$ cooling age of 11 Ma [Maluski et al., 1988; Fig. 1(c)]. The nearby Gophu La pluton appears somewhat older with Rb–Sr mica ages between 14.0 and 15.1 Ma (Ferrara et al., 1991). These ages indicate that intrusion of the Bhutan leucogranites is overall synchronous with the onset of exhumation of the HHC along the MCT at the end of the Mid-Miocene. This is in contrast with many other places along the MCT, where U–Pb intrusion ages of the leucogranites are significantly older than the $^{40}Ar/^{39}Ar$ cooling ages in the MCT (see below). Edwards and Harrison (1997) interpreted north–south extensional deformation along the STD to continue until 10 Ma from the offset observed within the Khula Gangri pluton. Thus, our data confirm the interpretation by other authors that the time of north–south extension is matched and outlasted by thrust motion along the MCT. This is interesting as the profile investigated here is much further east than other published profiles of Ar–Ar ages across the MCT.

7.1. Along strike age changes

The $^{40}Ar/^{39}Ar$ data presented above place a further constraint on the changes of age of metamorphism and exhumation along strike of the MCT. In central Nepal, Copeland et al. (1991, 2000) found muscovite cooling ages in the immediate hanging wall of the MCT of 3.8 ± 0.4 Ma. In the Langtang area, also in central Nepal, they are similarly young with 2.3 ± 0.4 to 8.9 ± 0.2 Ma (MacFarlane, 1993). In eastern central Nepal, Maluski et al. (1988) obtained no muscovite cooling ages from the MCT itself but present 5.7 ± 0.3 and 8.6 ± 0.3 ages from the hanging wall. These ages are in contrast to somewhat older ages of 12.0 ± 0.2 Ma from the Everest Transsect of the MCT zone in eastern Nepal (Hubbard and Harrison, 1989). The data from Hubbard and Harrison (1989) however, are very similar to the ones presented here. In the Annapurna region of western Nepal, Vannay and Hodges (1996) presented muscovite cooling ages around 14 and 15 Ma. In Pakistan, near the western syntaxis of the Himalaya, cooling ages are much older around 30 and 40 Ma (Zeitler, 1985). These ages appear to indicate that cooling and exhumation of the HHC occurred earlier near the syntaxes of the Himalaya than in the central part of the MCT. The lower temperature cooling history and final exhumation as revealed by the apatite fission track age of ~3 Ma is indistinguishable from that revealed in the Nepal section of the MCT (Copeland et al., 2000).

Interestingly, the ages presented here are closer to the intrusion ages of the leucogranites in the hanging wall than in most other places along strike of the MCT. In Zanskar, at Manaslu, at Shisha Pangma and at Makalu the Himalayan leucogranites have crystallisation ages no younger than 19 Ma (Edwards and Harrison, 1997 and references therein). Thus, cooling ages in the MCT are between 5 and 15 Ma younger than crystallisation of their respective leucogranites in the hanging wall.

8. Conclusion

$^{40}Ar/^{39}Ar$ age data from muscovite indicate cooling of the MCT between 11.2 Ma (direct hanging wall) and 14.1 Ma (400 m from hanging wall). These ages are repeated in two other samples 2.1 and 4.7 km in the hanging wall respectively, indicating that the MCT in the Tashigang transect is a zone in which several discrete packages of rocks are telescoped.

Older ages at larger distances from the hanging wall indicate that the exhumation rates increase with distance from the MCT. This is confirmed by preliminary *PT* estimates which indicate higher temperatures for the older samples. The highest estimated *PT* is around 650°C and 6.5 kbar. These data are consistent with the exhumation model of Grujic et al. (1996) in which the exhumation of the entire HHC is explained with a channel flow model.

Acknowledgements

M. and B. Regelsberger are thanked for their detailed sampling and geological descriptions of the rocks discussed herein. V. Stehlik is thanked for logistic support. D. Vance, M. Hubbart and B. Hacker are thanked for a series of suggestions on an earlier version of this manuscript. This project was supported by FWF project P-12846-GEO.

References

Avouac, J.P., Tapponier, P., 1993. Kinematic model of the active deformation in central Asia. Geophysical Research Letters 20, 895–898.

Brunel, M., Kienast, J.R., 1986. Etude petro-structurale des chevauchements ductile Himalayens sur la transversale de L'Everest-Makalu (Nepal oriental). Canadian Journal of Earth Sciences 23, 1117–1137.

Burchfield, B.C., Royden, L.H., 1985. North–south extension within the convergent Himalayan region. Geology 13, 679–682.

Burchfield, B.C., Chen, Z., Hodges, K.V., Liu, Y., Royden, L.H., Deng, C. et al., 1992. The south Tibetan detachment system, Himalayan Orogen:

extension contemporaneous with and parallel to shortening in a collisional mountain belt, Geological Society of America Special Paper 269.

Burg, J.P., Chen, G.M., 1984. Tectonics and structural zonation of southern Tibet. Nature 311, 219–223.

Copeland, P., Harrison, T.M., Hodges, K.V., Maruejol, P., Le Fort, P., Pecher, A., 1991. An early Pliocene thermal disturbance of the Main Central Thrust, central Nepal: implications for Himalayan Tectonics. Journal of Geophysical Research 96, 8475–8500.

Copeland, P., Le Fort, P., Henry, P., Man Rai, S., Foster, D., Parrish, R. et al., 2000. Neogene tectonothermal development of the Himalayan thrust system in the Kathmandu region, Nepal, Geological Society of America Bulletin (in press).

Davidson, D., Grujic, D., Hollister, L.S., Schmidt, S.M., 1997. Metamorphic reactions related to decompression and synkinematic intrusion of leucogranite, High Himalayan Crystallines, Bhutan. Journal of Metamorphic Geology 15, 593–612.

Edwards, M.A., Kidd, W.S.F., Li, J., Yue, Y., Clark, M., 1996. Multi-stage development of the southern Tibet detachment system near Khula Kangri. New data from Gonto La. Tectonophysics 260, 1–19.

Edwards, M.A., Harrison, T.M., 1997. When did the roof collapse? Late Miocene north–south extension in the high Himalaya revealed by Th–Pb monazite dating of the Khula Kangri granite. Geology 25, 543–546.

England, P.C., Molnar, P., 1993. The interpretation of inverted metamorphic isograds using simple physical calculations. Tectonics 12, 145–157.

Ferrara, G., Lombardo, B., Tonarini, S., Turi, B., 1991. Sr, Nd and O isotopic characterisation of the Gophu La and Gumburanjun leucogranites (High Himalaya). Schweizerische Mineralogische Petrographische Mitteilungen 71, 35–51.

Foster, D.A., Gleadow, A.J.W., 1996. Structural framework and denudation history of the flanks of the Kenya and Anza Rifts, East Africa. Tectonics 15, 258–271.

Foster, D.A., John, B.E., 1999. Quantifying tectonic exhumation in an extensional orogen with thermochronology: examples from the southern Basin and Range Province, Ring, U., Brandon, M., Lister, G.S., Willett, S.D., Exhumation Processes: Normal Faulting, Ductile Flow, and Erosion, Geological Society, London, Special Publication 154.

Foster, D.A., Gray, D.R., Bucher, M., 1999. Chronology of deformation within the turbidite-dominated Lachlan orogen: implications for the tectonic evolution of eastern Australia and Gondwana, Tectonics 18, 452–585.

Gansser, A., 1964. Geology of the Himalayas. Wiley Interscience, London.

Gansser, A., 1983. Geology of the Bhutan Himalaya. Denkschriften der Schweizerischen Naturforschenden Gesellschaft 96, 1–181.

Gleadow, A.J.W., Duddy, I.R., 1981. A natural long-term annealing experiment for apatite. Nuclear Tracks 5, 169–174.

Grujic, D., Casey, M., Davidson, C., Hollister, L., Kündig, R., Pavlis, T., et al., 1996. Ductile extrusion of the higher Himalayan Crystalline in Bhutan: evidence from quartz microfabrics. Tectonophysics 260, 21–44.

Harris, N., Massey, J., 1994. Decompression and anatexis of Himalayan metapelites. Tectonics 13, 1537–1546.

Harrison, T.M., Ryerson, F.J., Le Fort, P., Yin, A., Lovera, O.M., Catlos, E.J., 1997. A late Miocene–Pliocene origin for the Central Himalayan inverted metamorphism. Earth and Planetary Science Letters 146, 1–7.

Holland, T.J.B., Powell, R., 1990. An enlarged and updated internally consistent thermodynamic dataset with uncertainties and correlations: the system K_2O–Na_2O–CaO–MgO–FeO–Fe_2O_3–Al_2O_3–TiO_2–SiO_2–C–H_2–O_2. Journal of Metamorphic Geology 8, 89–124.

Hubbard, M.S., 1989. Thermobarometric constraints on the thermal history of the Main Central Thrust zone and Tibetan Slab, eastern Nepal Himalaya. Journal of Metamorphic Geology 7, 19–30.

Hubbard, M.S., Harrison, T.M., 1989. $^{40}Ar/^{39}Ar$ constraints on deformation and metamorphism in the Main Central Thrust zone and Tibetan Slab, eastern Nepal Himalaya. Tectonics 8, 865–880.

Jaupart, C., Provost, A., 1985. Heat focusing, granite genesis and inverted metamorphic gradients in continental collision zones. Earth and Planetary Science Letters 73, 385–399.

John, B.E., Foster, D.A., 1993. Structural and thermal constraints on the initiation angle of detachment faulting in the southern Basin and Range: the Chemehuevi Mountains case study. Geological Society of America Bulletin 105, 1091–1108.

Kirchner, D.L., Cosca, M.A., Masson, H., Hunziker, J.C., 1996. Staircase $^{40}Ar/^{39}Ar$ spectra of fine-grained white mica: timing and duration of deformation and empirical constraints on Argon diffusion. Geology 24, 747–750.

Le Fort, P., 1975. Himalaya: the collided range. Present knowledge of the continental arc. American Journal of Science 275, 1–44.

Le Fort, P., Pecher, A., Upreti, B.N., 1986. A section through the Tibetan slab in central Nepal (Kali Gandaki Valley): mineral chemistry and thermobarometry of the Main Central thrust zone. In: Le Fort, P., Colchen, C., Montenat, C. (Eds.), Sciences de la Terre Memoire 47. Foundation Scientifique de la Geologie et de ses Applications, pp. 211–228.

MacFarlane, A.M., 1993. Chronology of tectonic events in the crystalline core of the Himalaya, Langtang National Park, Central Nepal. Tectonics 12, 1004–1025.

Maluski, H., Matte, P., Brunel, M., Xusheng, X., 1988. $^{40}Ar/^{39}Ar$ dating of metamorphic and plutonic events in the north and high Himalaya belts (southern Tibet–China). Tectonics 7, 299–326.

Maruo, Y., Kizaki, K., 1983. Thermal structure in the nappes of the eastern Nepal Himalayas. In: Shams, F.A. (Ed.), Granites of the Himalaya, Karakorum and Hindu-Kush. Punjab University, Lahore, Pakistan, pp. 271–286.

McDougall, I., Harrison, T.M., 1988. Geochronology and Thermochronology by the $^{40}Ar/^{39}Ar$ Method. Oxford University Press, New York.

Molnar, P., England, P.C., 1990. Temperatures, heat flux and frictional stress near major thrust faults. Journal of Geophysical Research 95, 4833–4856.

Powell, R., Holland, T.J.B., 1988. An internally consistent thermodynamic dataset with uncertainties and correlations: 3 application to geobarometry worked examples and a computer program. Journal of Metamorphic Geology 6, 173–204.

Roddick, J.C., Cliff, R.A., Rex, D.C., 1980. The evolution of excess argon in Alpine biotites — A ^{40}Ar–^{39}Ar analysis. Earth and Planetary Science Letters 48, 185–208.

Searle, M.P., 1996. Cooling history, erosion, exhumation, and kinematics of the Himalaya–Karakorum–Tibet orogenic belt. In: Yin, A., Harrison, M. (Eds.), The Tectonic Evolution of Asia. Cambridge University Press, Cambridge, p. 641.

Swapp, S.M., Hollister, L.S., 1991. Inverted metamorphism within the Tibetan Slab of Bhutan: evidence for a tectonically transported heat-source. Canadian Mineralogist 29, 1019–1041.

Vannay, J.C., Hodges, K.V., 1996. Tectonometamorphic evolution of the Himalayan metamorphic core between the Annapurna and Dhaulagiri, central Nepal. Journal of Metamorphic Geology 14, 635–656.

Zeitler, P.K., 1985. Cooling history of the NW Himalaya, Pakistan. Tectonics 4, 127–151.